Polymer Chemistry

Accepted Manuscript

ROYAL SOCIETY OF CHEMISTRY

www.rsc.org/polymers

Journal Name

ARTICLE

Macro-RAFT agent mediated dispersion polymerization: the monomer concentration effect on the morphology of the *in situ* synthesized block copolymer nano-objects

Zhonglin Ding, Chengqiang Gao, Shuang Wang, Hui Liu and Wangqing Zhang*

Received 00th January 20xx,

Accepted 00th January 20xx

DOI: 10.1039/x0xx00000x

www.rsc.org/

Abstract: The monomer concentration affecting the morphology of the *in situ* synthesized block copolymer nano-objects during the macro-RAFT agent mediated dispersion polymerization is investigated. It is found that the monomer concentration exerts great influence on both the polymerization kinetics of the poly(ethylene glycol) trithiocarbonate macro-RAFT agent mediated dispersion polymerization and the morphology of the *in situ* synthesized nano-objects of the poly(ethylene glycol)-*block*-polystyrene (PEG-*b*-PS) diblock copolymer. The poly(ethylene glycol) trithiocarbonate macro-RAFT agent mediated dispersion polymerization of styrene in the alcoholic solvent at 50% high monomer concentration follows similar kinetic behaviour to homogeneous RAFT polymerization as indicated by the linear $\ln([M]_0/[M])$-time plot, and the good control both on the molecular weight of the PEG-*b*-PS diblock copolymer and the molecular weight distribution is achieved. With the extension of the PS block, the morphology of the *in situ* synthesized PEG-*b*-PS nano-objects changes from the porous nanospheres to the bicontinuous nanospheres and finally to the entrapped vesicles, which is much different from the dispersion RAFT polymerization under low monomer concentration. Our results demonstrate that the monomer concentration is an important parameter affecting the morphology of the *in situ* synthesized block copolymer nano-objects.

1 Introduction

Block copolymer nano-assemblies with well-defined morphology have gained great attention in the past decade due to their potential applications.[1-3] In the last thirty years or so, the micellization of amphiphilic block copolymer in the block-selective solvent has been widely documented,[4-30] and the convenience of this micellization strategy to form amphiphilic block copolymer nano-objects is demonstrated. Recently, the polymerization-induced self-assembly (PISA) offers a potential option for the *in situ* synthesis of block copolymer nano-objects through the macro-RAFT agent mediated polymerization under emulsion or dispersion condition.[31-35] Compared with the micellization of the pre-synthesized block copolymers in the block-selective solvent, the PISA strategy has two advantages. First, the preparation of the block copolymer nano-objects is achieved simultaneously just at the RAFT synthesis of the block copolymer, and therefore no additional procedures such as the dissolution of the block copolymer in a common solvent and then the micellization triggering usually by adding a block-selective solvent are needed. Second, the PISA strategy affords the *in situ* synthesis of concentrated block copolymer nano-objects with the block copolymer concentration as high as 30 wt%, which is much beyond that in the micellization strategy. Up to now, following this PISA strategy, block copolymer nano-objects with various morphologies such as spheres, worms or rods and vesicles have been efficiently generated in non-aqueous or aqueous dispersion during the RAFT synthesis of amphiphilic block copolymers.[36-61]

In the macro-RAFT agent mediated dispersion polymerization, all polymerization ingredients including the macro-RAFT agent, the initiator and the monomer are dissolved in the solvent in the initial polymerization stage. With the proceeding of the RAFT polymerization, the insoluble block of the synthesized amphiphilic block copolymer extends to a critical point at which the self-assembly of the *in situ* synthesized amphiphilic block copolymer into micelles takes place. After this onset of micellization of the *in situ* synthesized block copolymer, the subsequent dispersion RAFT polymerization occurs dominantly in the monomer-swollen micelles, and the further extension of the insoluble block in the block copolymer micelles leads to either the growth in the size or the morphology transition of the block copolymer nano-objects. It has been demonstrated that,[35] several parameters listed below are found to dictate the size and morphology of the *in situ* synthesized block copolymer nano-

[a] *Key Laboratory of Functional Polymer Materials of the Ministry of Education, Collaborative Innovation Center of Chemical Science and Engineering (Tianjin), Institute of Polymer Chemistry, Nankai University, Tianjin 300071, China.*
[b] *E-mail: wqzhang@nankai.edu.cn; Fax: 86-22-23503510.*
† Electronic Supplementary Information (ESI) available: See DOI: 10.1039/x0xx00000x

objects. First, the polymerization degree (DP) of the solvophobic block is found to be firmly correlative to the morphology of the *in situ* synthesized block copolymer nano-objects, and the morphology of the block copolymer nano-objects usually undergoes the transition from nanospheres to worms and finally to vesicles with the increasing DP of the solvophobic block during the dispersion RAFT polymerization.[47-60] Second, the chain length of the macro-RAFT agent, which forms the solvophilic block of the *in situ* synthesized block copolymer, also exerts great influence on the morphology of the block copolymer nano-objects.[52-58] It is found that, the long macro-RAFT agent leads favorably to block copolymer nanospheres and the short macro-RAFT agent leads favorably to block copolymer vesicles. Besides, the solvent character of the polymerization medium and the concentration of the feeding monomer are also found to exert influence on the morphology of the *in situ* synthesized block copolymer nano-objects.[46,56-58] By tuning the aforementioned parameters, block copolymer nano-objects with various morphologies such as nanospheres, nanorods, nanowires, and vesicles were prepared through dispersion RAFT polymerization.[47-60] Compared with the numerous reports on the block copolymer composition affecting the morphology of the block copolymer nano-objects,[47-60] the monomer concentration affecting the morphology of the *in situ* synthesized block copolymer nano-objects during the dispersion RAFT polymerization is inappropriately neglected,[56,57] although it is revealed that some interesting block copolymer morphologies such as multi-layered vesicles has been prepared at 50 wt% concentrated monomer concentration under dispersion condition.[44]

In this study, the poly(ethylene glycol) trithiocarbonate macro-RAFT agent mediated dispersion polymerization of styrene in the alcoholic solvent under different monomer concentration is performed, and the monomer concentration affecting the morphology of the *in situ* synthesized nano-objects of the poly(ethylene glycol)-*block*-polystyrene (PEG-*b*-PS) diblock copolymer is investigated. It is found that the monomer concentration is crucial to determine the morphology of the *in situ* synthesized PEG-*b*-PS diblock copolymer nano-objects. That is, the PEG-*b*-PS nanospheres are formed under diluted monomer concentration (10 wt%), and the cavitated nano-objects including vesicles, porous nanospheres and bicontinuous nanospheres are prepared under concentrated monomer concentration (20-50 wt%). To the best of our knowledge, the block copolymer morphology of the porous nanospheres and the bicontinuous nanospheres have not been detected experimentally under PISA conditions, although it is hypothetically expected by simulation.[62] Our results suggest the crucial role of the monomer concentration on the morphology of the *in situ* synthesized block copolymer nano-objects under PISA conditions.

2 Experimental

2.1 Materials

Styrene (St, >98%, Tianjin Chemical Company) was distilled under reduced pressure prior to use. 2,2'-Azobis(isobutyronitrile) (AIBN, >99%, Tianjin Chemical Company) was recrystallized from ethanol before being used. The macro-RAFT agent of poly(ethylene glycol) trithiocarbonate (PEG_{45}-TTC, in which the subscript represents the number of the repeated unit and TTC represents the RAFT terminal of trithiocarbonate) was synthesized as reported previously.[55] All the other chemical reagents of analytical grade were purified by standard procedures or used as received. Deionized water was used in the present experiment.

2.2 Dispersion RAFT polymerization and synthesis of the PEG-*b*-PS diblock copolymer nano-objects

The PEG_{45}-TTC macro-RAFT agent mediated dispersion polymerization of styrene was carried out in the ethanol/water mixture (80/20, w/w) at 70 °C with the weight ratio of the styrene monomer to the solvent ranging from 10% to 50%, in which the molar ratio of $[St]_o$:$[mPEG_{45}\text{-}TTC]_o$:$[AIBN]_o$ was kept constant at 1200:3:1. Herein, a typical dispersion RAFT polymerization with the weight ratio of the styrene monomer to the polymerization solvent at 50% is introduced. Into a 25 mL Schlenk flask with a magnetic bar, PEG_{45}-TTC (0.113 g, 0.0480 mmol), St (2.00 g, 19.2 mmol), and AIBN (2.63 mg, 0.00160 mmol) dissolved in the 80/20 ethanol/water mixture (2.11 g) were added. The mixture was degassed with nitrogen at 0 °C and then the polymerization was initiated by immersing the flask into a preheated oil bath at 70 °C. After a given time, the polymerization was quenched by immersing the flask in iced water. The monomer conversion was detected by UV-vis analysis as discussed elsewhere,[45] in which a given volume of the colloidal dispersion (ca. 1.0 mL) was filtered twice with a 0.22 μm nylon filter, and then the filtrate was diluted with ethanol and analyzed at 245 nm. To detect the morphology of the *in situ* synthesized PEG-*b*-PS diblock copolymer nano-objects, a small drop of the colloidal dispersion was initially diluted with suitable amount of the 80/20 ethanol/water mixture, and then a drop of the colloidal dispersion was deposited onto a piece of a copper grid, dried under vacuum at room temperature, and finally observed by transmission electron microscope (TEM). To collect the PEG-*b*-PS diblock copolymer for the GPC and ^{1}H NMR analysis, the colloidal dispersion was centrifuged (12500 r/min, 10 min), washed with methanol (10 mL × 3), and then dried under vacuum at room temperature to afford the block copolymer powder.

2.3 Characterization

The ^{1}H NMR analysis was performed on a Bruker Avance III 400 MHz NMR spectrometer using $CDCl_3$ as the solvent. The molecular weight and its distribution or the polydispersity index (PDI, PDI = M_w/M_n) of the synthesized polymer were determined by gel permeation chromatography (GPC) analysis using a Waters 600E GPC system equipped with three TSK-GEL columns and a Waters 2414 refractive index detector, where THF was used as the eluent at flow rate of 0.6 mL/min at 30.0 °C and the narrow-polydispersity polystyrene was used as the calibration standard. The UV-vis analysis was performed on

a Varian 100 UV-vis spectrophotometer. TEM observation was performed using a Tecnai G^2 F20 electron microscope at an acceleration of 200 kV.

3 Result and discussion

3.1 Synthesis of the PEG_{45}-TTC macro-RAFT agent

The macro-RAFT agent of PEG_{45}-TTC was prepared by esterification reaction of the hydroxyl terminal in PEG_{45}-OH with the carboxyl group in *S*-1-dodecyl-*S*′-(α,α′-dimethyl-α′′-acetic acid) trithiocarbonate (DDMAT) as shown in Figure 1A as discussed elsewhere.[55] From the ^{1}H NMR spectra shown in Figure 1B, all the proton signals are nicely assigned, and therefore the chemical structure of PEG_{45}-TTC is confirmed. By comparing the signals at 1.10-1.45 ppm (b) and at 3.61-3.70 ppm (g), the molecular weight $M_{n,NMR}$ of PEG_{45}-TTC at 2.3 kg/mol is obtained. From the GPC traces shown in Figure 1C, the molecular weight $M_{n,GPC}$ of PEG_{45}-TTC at 3.1 kg/mol with the PDI value at 1.04 is obtained. It is found that the $M_{n,NMR}$ of the PEG_{45}-TTC macro-RAFT agents is slightly smaller than $M_{n,GPC}$, and the reason is possibly ascribed to the PS standard used in the GPC analysis.

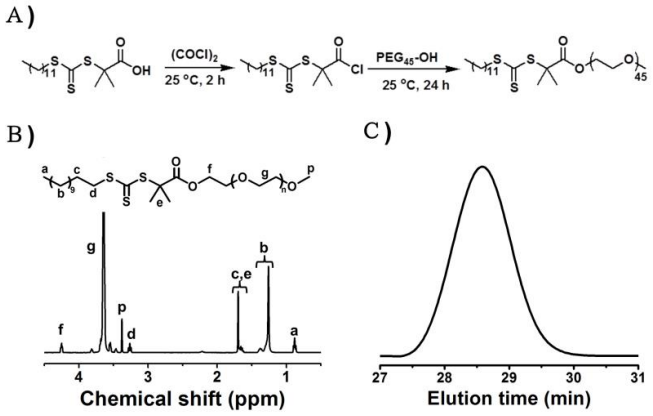

Fig 1. Synthesis of PEG_{45}-TTC (A), the ^{1}H NMR spectra (B) and GPC traces (C) of PEG_{45}-TTC.

3.2 The dispersion RAFT polymerization under different monomer concentration and the morphology of the *in situ* synthesized diblock copolymer

The PEG_{45}-TTC macro-RAFT agent mediated dispersion polymerization of styrene was performed in the ethanol/water mixture (80:20 by weight) under $[St]_o$:$[PEG_{45}\text{-TTC}]_o$:$[AIBN]_o$ = 400:1:0.333. The alcoholic solvent of the 80/20 ethanol/water mixture is chosen because it is a good solvent of the styrene monomer and the PEG_{45}-TTC macro-RAFT agent, but a non-solvent of the PS block of the PEG-*b*-PS diblock copolymer, which is essential for the self-assembly of the PEG-*b*-PS diblock copolymer in the solvent. With the proceeding of the RAFT polymerization, the PS block in the PEG-*b*-PS diblock copolymer becomes insoluble in the alcoholic solvent, which is indicated by the cloudy dispersion at the polymerization time of 6-7 h depended on the monomer concentration, and then the *in situ* synthesized PEG-*b*-PS diblock copolymer self-assembles into nano-objects in the alcoholic solvent.

To check the monomer concentration affecting the morphology of the PEG-*b*-PS diblock copolymer, the dispersion RAFT polymerization with constant $[St]_o$:$[PEG_{45}\text{-TTC}]_o$:$[AIBN]_o$ but at the different monomer concentration ranging from 10% to 60% was checked (note: the monomer concentration was defined by the weight ratio of the styrene monomer to the solvent herein and in the subsequent discussion). The dispersion RAFT polymerization with the monomer concentration above 60% was not checked, since the PEG-*b*-PS diblock copolymer could not be dispersed in the solvent and some precipitate was observed during the RAFT polymerization. The PEG-*b*-PS nano-objects formed at the monomer concentration below 50% were dispersed uniformly in the polymerization medium, since no or just very slight precipitation was observed. The morphology of these PEG-*b*-PS nano-objects prepared by the dispersion RAFT polymerization both at moderate monomer conversion of 50-60% and at high monomer conversion above 93% was checked. Figure 2 summarizes the TEM images of the PEG-*b*-PS diblock copolymer nano-objects synthesized at moderate monomer conversion. As shown in Figure 2, at the six cases of the monomer concentration ranging from 10% to 60%, the nanospheres with the average size at 35±2 nm (Figure 2A), the mixture of 98±12 nm vesicles and 130±30 nm porous nanospheres (Figure 2B), the major of 138±45 nm porous nanospheres as well as few of 74±15 nm vesicles (Figure 2C), 160±60 nm porous nanospheres (Figures 2D and 2E), and the major of 368±100 nm porous nanospheres as well as some of 168±35 nm porous nanospheres (Figures 2F and 2G), and the large-sized aggregates up to 2 μm with the bicontinuous structure (Figures 2H and 2I) are formed, respectively. These PEG-*b*-PS diblock copolymers with different morphology have very similar theoretical molecular weight according to eq 1 as discussed elsewhere,[63] which is shown by the insets in the TEM images. The GPC analysis of the PEG-*b*-PS diblock copolymers also confirms the similar molecular weight of the six PEG-*b*-PS diblock copolymers with narrow distribution (PDI < 1.12), although the slight shoulder at the high molecular side is observed in the case of high monomer concentration (Figure 3). Clearly, these results suggest that the monomer concentration exerts great influence on the morphology of the *in situ* synthesized PEG-*b*-PS nano-objects.

To further confirm the monomer concentration affecting the morphology of the *in situ* synthesized PEG-*b*-PS nano-objects, the dispersion RAFT polymerization underwent till the high monomer conversion up to 93% was achieved (note: the dispersion RAFT polymerization at the 50% monomer concentration run a little slow and 89.0% monomer conversion was obtained even the polymerization was extended to 48 h). This dispersion RAFT polymerization at high monomer conversion eliminates or decreases the effect of the residual monomer on the morphology of the *in situ* synthesized PEG-*b*-PS nano-objects. As shown in Figure 4, although the five

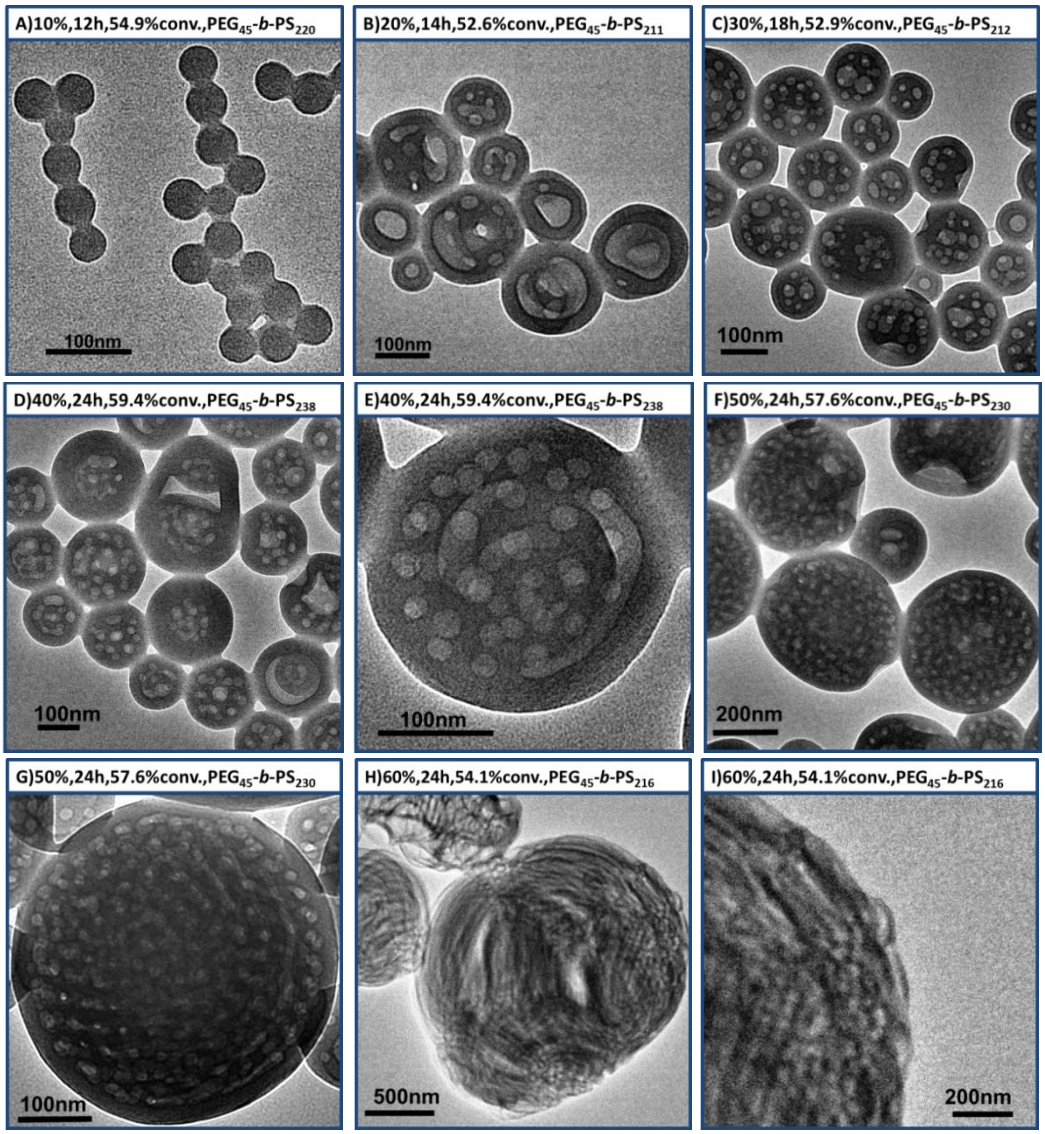

Fig 2. The TEM images of the PEG-*b*-PS nano-objects formed at the monomer concentration at 10% (A), 20% (B), 30% (C), 40% (D and E), 50% (F and G), and 60% (H and I) at the 50~60% moderate monomer conversion. Insets: the polymerization time, the monomer conversion, and the chemical composition of the PEG-*b*-PS diblock copolymer.

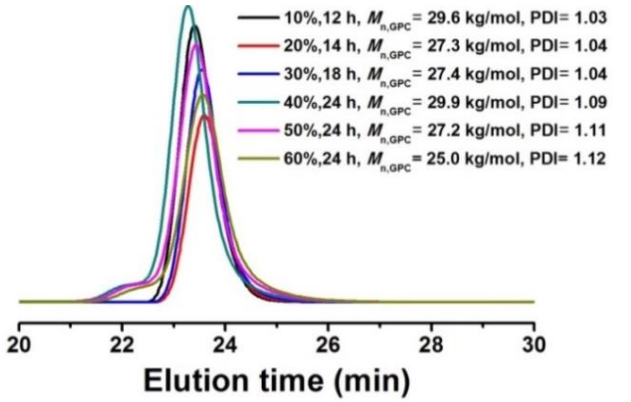

Fig 3. The GPC traces of the PEG_{45}-*b*-PS diblock copolymers synthesized at different monomer concentration at the 50~60% moderate monomer conversion.

diblock copolymers of PEG-*b*-PS have the similar molecular weight (Figure S1) at the five cases of the St monomer concentration, nanospheres were formed at low monomer concentration of 10% (Figure 4A), vesicles were formed at moderate monomer concentration of 20-30% (Figures 4B and 4C), and the complex morphology of entrapped vesicles[51] was formed at the high monomer concentration of 40-50% (Figures 4D-F), respectively. These results confirm that the monomer concentration is an important parameter affecting the morphology of the *in situ* synthesized PEG-*b*-PS nano-objects. Furthermore, by comparing the block copolymer morphologies shown in Figures 2 and 4, it is found that the morphology of the PEG-*b*-PS nano-objects prepared at moderate monomer conversion is much different from those prepared at high monomer conversion. This is partly ascribed to the different block length of the solvophobic PS block in the PEG-*b*-PS diblock copolymer. It has been reported that either the size of the *in situ* synthesized block copolymer nano-objects increases

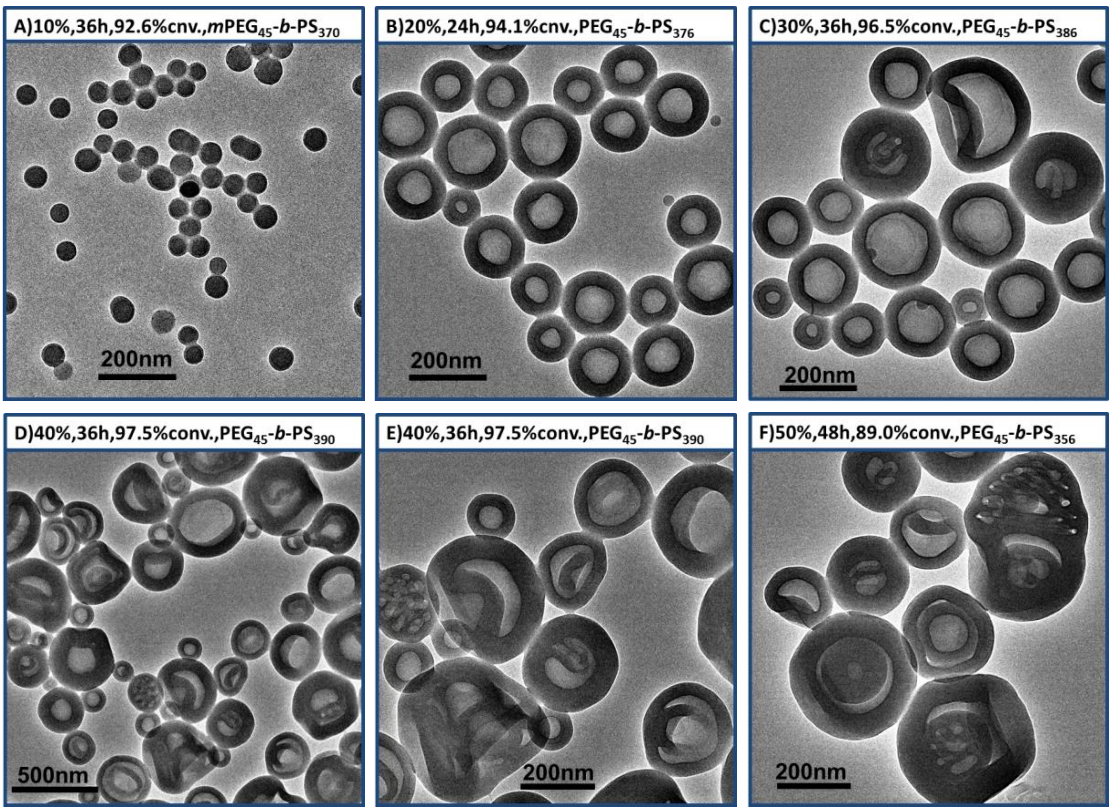

Fig 4. The TEM images of the PEG-*b*-PS nano-objects formed at the monomer concentration at 10% (A), 20% (B), 30% (C), 40% (D and E), and 50% (F) at the 93-97% high monomer conversion. Insets: the polymerization time, the monomer conversion, and the chemical composition of the PEG-*b*-PS diblock copolymer.

or the morphology of the block copolymer nano-objects undergoes the evolution from spheres to worms and finally to vesicles with the extension of the solvophobic block.[47-60] However, in the present dispersion RAFT polymerization especially at high monomer concentration, the thing is much different. For example, in the case of 50% monomer concentration, the PEG-*b*-PS diblock copolymer morphology changes from the PEG_{45}-*b*-PS_{230} porous microspheres (Figure 2F) to the PEG_{45}-*b*-PS_{356} entrapped vesicles (Figure 4F) when the DP of the PS block increases from 230 to 356. Generally, the exact reason to dictate the block copolymer morphology under PISA condition is very complex, and not only the block copolymer itself but also the solvent condition including the solvent character, the temperature and the monomer dissolved in the solvent can affect the morphology of the *in situ* synthesized block copolymer nano-objects.[35] In the present dispersion RAFT polymerization at high monomer concentration, the concentrated monomer, which is a solvent for the PS block of the PEG-*b*-PS diblock copolymer or a plasticizer for the *in situ* synthesized PEG-*b*-PS nano-objects, greatly changes the solvent character and therefore exerts somewhat influence on the morphology of the PEG-*b*-PS nano-objects, although the exact reason needs further study.

3.3 The kinetics of the dispersion RAFT polymerization and the PEG-*b*-PS morphology evolution during the RAFT polymerization

The porous nanospheres of the PEG-*b*-PS diblock copolymer are one of the new morphology under PISA conditions. This arouses our interest to explore how these porous nanospheres being formed during the dispersion RAFT polymerization. To check how these porous nanospheres being formed, herein the polymerization kinetics of the typical dispersion RAFT polymerization under $[St]_o$:$[PEG_{45}$-$TTC]_o$:$[AIBN]_o$ = 400:1:0.333 with the monomer concentration at 50% was explored and the morphology of the *in situ* synthesized PEG-*b*-PS nano-objects was checked.

As shown in Figure 5A, the PEG_{45}-TTC macro-RAFT agent mediated dispersion polymerization ran smoothly and 89% monomer conversion was achieved in 48 h. The further increase in the polymerization time just led to a very slight increase in the monomer conversion. From Figure 5B, the linear $\ln([M]_0/[M])$-time plot is observed, which suggests that the PEG_{45}-TTC macro-RAFT agent mediated RAFT polymerization at 50% monomer concentration undergoes a polymerization kinetics just like a general homogeneous RAFT polymerization.[64] For a macro-RAFT agent mediated dispersion polymerization of styrene in the alcoholic solvent at moderate monomer concentration of 10-20%, a two-stage $\ln([M]_0/[M])$-time plot containing a gradient linear stage corresponding to the initial homogeneous polymerization and a steep linear one corresponding to the later heterogeneous polymerization was usually observed.[55,57,59,60] This two-stage polymerization kinetics is also found in the present dispersion RAFT polymerization at 10% monomer concentration (Figure S2). Clearly, the kinetics of the present dispersion RAFT

polymerization at 50% high monomer conversion is much different. The reason is possibly due to the fed monomer with high monomer concentration, which greatly changes the solvent character. Since the styrene monomer is a solvent for the PS block of the PEG-*b*-PS block copolymer, the feeding styrene monomer with high concentration will greatly increase the solubility of the PEG-*b*-PS diblock copolymer in the styrene/ethanol/water mixture, which makes the dispersion RAFT polymerization to undergo similarly with a homogeneous RAFT polymerization. The PEG-*b*-PS diblock copolymers synthesized at different polymerization time are characterized by GPC analysis and ^{1}H NMR analysis (Figure 5C and Figure S3). The molecular weight $M_{n,NMR}$ of the PEG-*b*-PS diblock copolymer is calculated by comparing the area ratio of the characteristic chemical shift at δ = 6.31~7.25 ppm (j, l, k) of the methyl group in the PS block to that of the protons of ethyl at δ = 3.61-3.70 ppm (g) in the PEG block, and the results are summarized in Figure 5D. Based on the GPC analysis, the molecular weight $M_{n,GPC}$ of the PEG_{45}-*b*-PS diblock copolymer and its distribution index of PDI are obtained and summarized in Figure 5D. The theoretical molecular weight $M_{n,th}$ of the PEG_{45}-*b*-PS block copolymer is also calculated by the monomer conversion following eq 1. It is found that the three molecular weight values of the PEG_{45}-*b*-PS diblock copolymer, $M_{n,NMR}$, $M_{n,th}$, and $M_{n,GPC}$, are close to each other. Furthermore, all the PEG_{45}-*b*-PS diblock copolymers synthesized at different polymerization time have a narrow molecular weight distribution as indicated by the low PDI at 1.05-1.11, although a slight shoulder at the higher molecular weight side is detected at the case of high monomer conversion. This shoulder is possibly ascribed to the slight bimolecular radical termination in the RAFT polymerization at the high monomer conversion as discussed elsewhere.[57] All together, these results suggest that the PEG_{45}-TTC macro-RAFT mediated dispersion polymerization affords good control both on the PEG-*b*-PS diblock copolymer molecular weight and on the molecular weight distribution.

$$M_{n,th} = \frac{[monomer]_0 \times M_{monomer}}{[RAFT]_0} \times conversion + M_{RAFT} \quad (1)$$

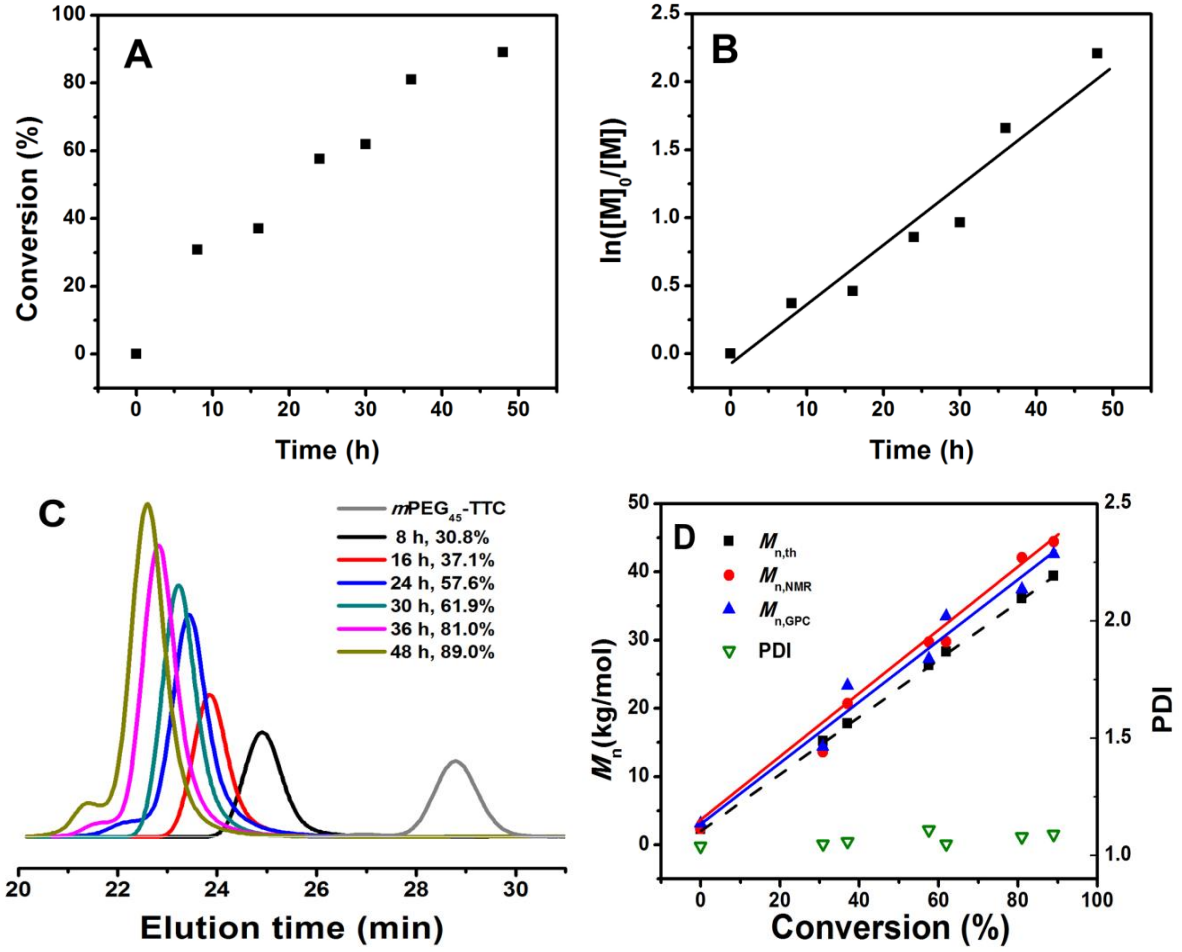

Fig 5. The monomer conversion-time plot (A) and the ln([M]0/[M])-time plot (B) for the PEG_{45}-TTC macro-RAFT agent mediated dispersion polymerization at 50% monomer concentration, the GPC traces (C) and the molecular weight and PDI of the PEG-*b*-PS diblock copolymer prepared through the dispersion RAFT polymerization at different monomer conversion (D).

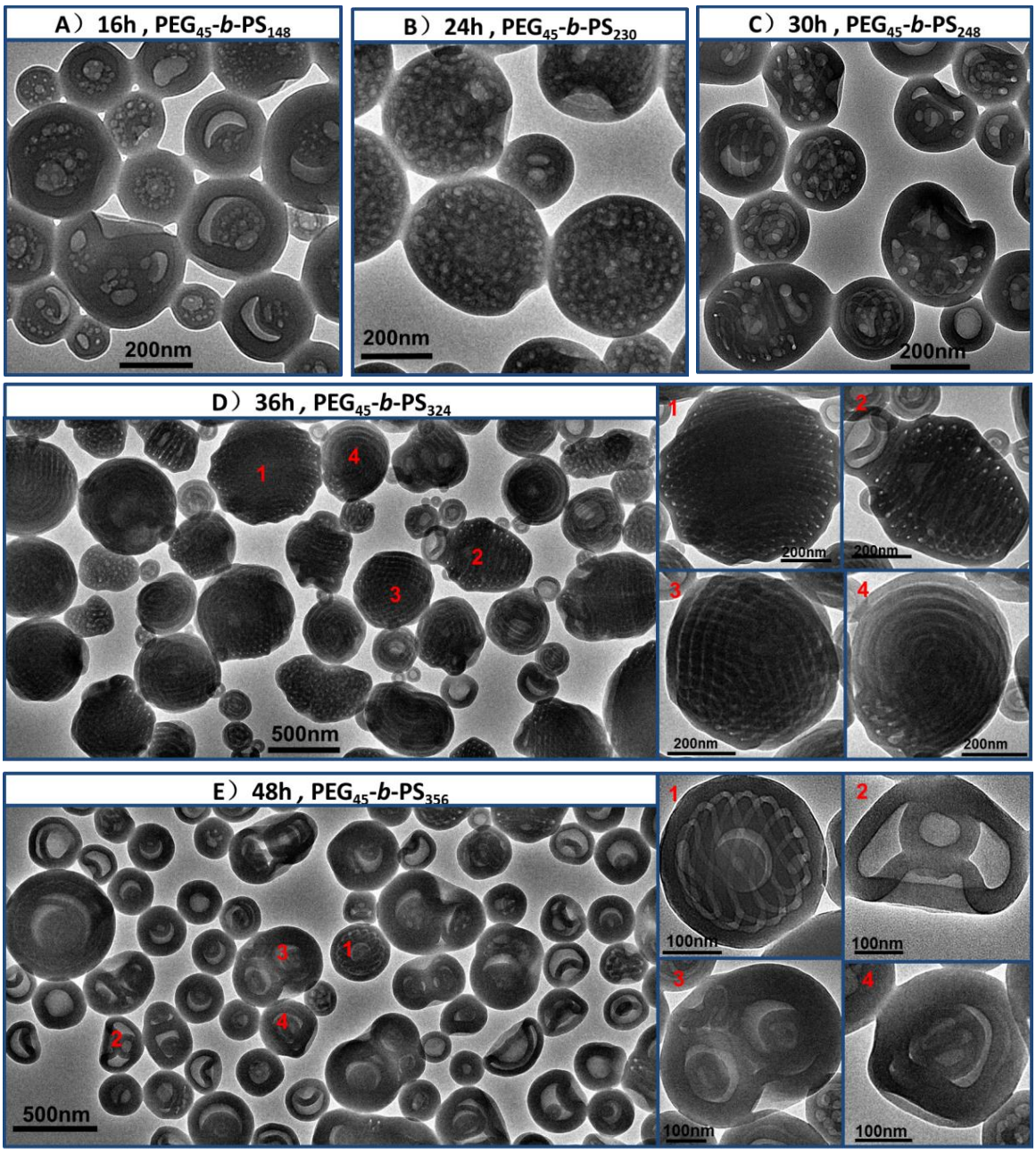

Fig 6. TEM images the PEG-*b*-PS nano-objects prepared through the dispersion RAFT polymerization at 50% monomer concentration at different polymerization time of 16 h (A), 24 h (B), 30 h (C), 36 h (D) and 48 h (E).

The *in situ* synthesized PEG_{45}-*b*-PS diblock copolymer nano-objects through the dispersion RAFT polymerization at different polymerization time are checked by TEM, and the TEM images are summarized in Figure 6. To clearly evaluate the DP of the newly formed PS block affecting the PEG_{45}-*b*-PS diblock copolymer morphology, the detailed composition of the PEG-*b*-PS diblock copolymers is indicated as insets in the TEM images. Note: the polymerization mixture becomes turbid at 6 h at 23.4% monomer conversion, and therefore just the PEG-*b*-PS diblock copolymer morphology after the onset of micellization is checked. As shown in Figures 6A, B and C, porous nanospheres of PEG-*b*-PS are formed at the 37-62% monomer conversion with the polymerization time ranging from 16 to 30 h. With the increasing DP of the PS block, the average size of the porous nanospheres increases from 190 to 290 nm. At the case of 81% monomer conversion in 36 h, the morphology of the *in situ* synthesized PEG-*b*-PS diblock copolymer nano-objects changes greatly, and the majority of the four kinds of the bicontinuous nanospheres as indicated by 1, 2, 3 and 4,[23-26,62] and few of 180±40 nm vesicles are formed (Figure 6D). By checking the high-resolution TEM images of the bicontinuous nanospheres, the inner structure in the 1, 2 and 3 bicontinuous nanospheres is just slightly different, whereas the 4 bicontinuous nanospheres are somewhat like the multilayer vesicles.[44] At the case of 89% monomer conversion in 48 h, entrapped vesicles are formed (Figure 6E). By carefully

checking the entrant in the vesicles, four entrapped vesicles of 1, 2, 3 and 4 as shown by the high-resolution TEM images are classified. In the general macro-RAFT agent mediated dispersion RAFT polymerization at low or moderate monomer conversion, the morphology evolution from nanospheres to worms and finally to vesicles have been found,[47-60] and the reason is ascribed to the increasing interfacial curvature between the solvophilic and solvophobic blocks with the extension of the solvophobic block during the RAFT polymerization. Clearly, the present PEG_{45}-TTC macro-RAFT agent mediated dispersion polymerization at high monomer concentration affords new morphology of the PEG-*b*-PS diblock copolymer including the porous nanospheres, the bicontinuous nanospheres and the entrapped vesicles, which is much different from the dispersion RAFT polymerization under low or moderate monomer concentration. It is believed that, although the exact reason on how the PEG-*b*-PS diblock copolymer nano-objects with new morphology being formed needs further study, the macro-RAFT agent mediated dispersion polymerization of concentrated monomer may be a promising method to fabricate new morphology of block copolymer nano-assemblies.

4 Conclusions

The PEG_{45}-TTC macro-RAFT agent mediated dispersion polymerization of styrene in the alcoholic solvent with different monomer concentration is investigated. It is found that the monomer concentration exerts great influence on the morphology of the *in situ* synthesized nano-objects of the PEG-*b*-PS diblock copolymer. At the case of low monomer concentration, spherical nanoparticles of the PEG-*b*-PS diblock copolymer are formed in the PEG_{45}-TTC macro-RAFT agent mediated dispersion polymerization; at the case of moderate monomer concentration, vesicles are formed; at the case of high monomer concentration, entrapped vesicles are formed, respectively. The polymerization kinetics of the macro-RAFT agent mediated dispersion polymerization at 50% high monomer concentration is investigated and the morphology of the *in situ* synthesized PEG-*b*-PS nano-objects in the dispersion RAFT polymerization is checked. It is found that the PEG_{45}-TTC macro-RAFT agent mediated dispersion polymerization at 50% high monomer concentration undergoes the kinetic similar with a homogeneous RAFT polymerization, as indicated by the linear $\ln([M]_0/[M])$-time plot, and the good control both in the molecular weight of the PEG-*b*-PS diblock copolymer and the molecular weight distribution is achieved. It is found that, with the extension of the PS block of the PEG-*b*-PS diblock copolymer, the morphology of the *in situ* synthesized diblock copolymer nano-objects changes from the porous nanospheres to the bicontinuous nanospheres and finally to the entrapped vesicles, which is much different from the dispersion RAFT polymerization under low or moderate monomer concentration. Our results demonstrate that the monomer concentration is an important parameter affecting the morphology of the *in situ* synthesized block copolymer nano-objects under PISA conditions, which is somewhat neglected previously.

Acknowledgements

The financial support by National Science Foundation of China (№ 21274066 and 21474054), PCSIRT (IRT1257), and NFFTBS (№ J1103306) is gratefully acknowledged.

Notes and references

1 Y. Mai and A. Eisenberg, *Chem. Soc. Rev.*, 2012, **41**, 5969-5985.
2 S. J. Holder and N. A. J. M. Sommerdijk, *Polym. Chem.* 2011, **2**, 1018-1028.
3 M. J. Monteiro and M. F. Cunningham, *Macromolecules*, 2012, **45**, 4939-4957.
4 K. Yu, C. Bartels, A. Eisenberg, *Langmuir*, 1999, **15**, 7157-7167.
5 T. Azzam and A. Eisenberg, *Angew. Chem. Int. Ed.*, 2006, **45**, 7443-7447.
6 H. Cui, Z. Chen, S. Zhong, K. L. Wooley and D. J. Pochan, *Science*, 2007, **317**, 647-650.
7 N. P. Truong, J. F. Quinn, M. V. Dussert, N. B. T. Sousa, M. R. Whittaker and T. P. Davis, *ACS Macro Lett.*, 2015, **4**, 381-386.
8 R. Fenyves, M. Schmutz, I. J. Horner, F. V. Bright and J. Rzayev, *J. Am. Chem. Soc.*, 2014, **136**, 7762-7770.
9 M. J. Barthel, U. Mansfeld, S. Hoeppener, J. A. Czaplewska, F. H. Schacher and U. S. Schubert, *Soft Matter*, 2013, **9**, 3509-3520.
10 R. T. Pearson, N. J. Warren, A. L. Lewis, S. P. Armes and G. Battaglia, *Macromolecules*, 2013, **46**, 1400-1407.
11 C. Herfurth, P. M. de Molina, C. Wieland, S. Rogers, M. Gradzielski and A. Laschewsky, *Polym. Chem.*, 2012, **3**, 1606-1617.
12 W. Kim, J. Thvenot, E. Ibarboure, S. Lecommandoux and E. L. Chaikof, *Angew. Chem. Int. Ed.*, 2010, **49**, 4257-4260.
13 A. J. de Graaf, K. W. M. Boere, J. Kemmink, R. G. Fokkink, C. F. van Nostrum, D. T. S. Rijkers, J. van der Gucht, H. Wienk, M. Baldus, E. Mastrobattista, T. Vermonden and W. E. Hennink, *Langmuir*, 2011, **27**, 9843-9848.
14 I. C. Reynhout, J. J. L. M. Cornelissen and R. J. M. Nolte, *J. Am. Chem. Soc.*, 2007, **129**, 2327-2332.
15 J. B. Gilroy, D. J. Lunn, S. K. Patra, G. R. Whittell, M. A. Winnik and I. Manners, *Macromolecules*, 2012, **45**, 5806-5815.
16 F. F. Taktak and V. Bütün, *Polymer*, 2010, **51**, 3618-3626.
17 C. Pietsch, U. Mansfeld, C. Guerrero-Sanchez, S. Hoeppener, A. Vollrath, M. Wagner, R. Hoogenboom, S. Saubern, S. H. Thang, C. R. Becer, J. Chiefari and U. S. Schubert, *Macromolecules*, 2012, **45**, 9292-9302.
18 W. Zhao, D. Chen, Y. Hu, G. M. Grason and T. P. Russell, *ACS Nano*, 2010, **5**, 486-492.
19 Y. He, Z. Li, P. Simone and T. P. Lodge, *J. Am. Chem. Soc.*, 2006, **128**, 2745-2750.
20 V. A. Vasantha, S. Jana, S. S.-C. Lee, C.-S. Lim, Serena L.-M. Teo, A. Parthiban and J. G. Vancso, *Polym. Chem.*, 2015, **6**, 599-606.

21 J. Dupont, G. Liu, K. Niihara, R. Kimoto and H. Jinnai, *Angew. Chem. Int. Ed.*, 2009, **48**, 6144-6147.
22 Z. Ge and S. Liu, *Macromol. Rapid Commun.* 2009, **30**, 1523-1532.
23 K. Yu, L. F. Zhang and A. Eisenberg, *Langmuir*, 1996, **12**, 5980-5984.
24 K. Hales, Z. Chen, K. L. Wooley and D. J. Pochan, *Nano Lett.*, 2008, **8**, 2023-2026.
25 B. E. McKenzie, H. Friedrich, M. J. M. Wirix, J. F. de Visser, O. R. Monaghan, P. H. H. Bomans, F. Nudelman, S. J. Holder and N. A. J. M. Sommerdijk, *Angew. Chem. Int. Ed.*, 2015, **54**, 2457-2461.
26 S. A. Barnhill, N. C. Bell, J. P. Patterson, D. P. Olds, and N. C. Gianneschi, *Macromolecules*, 2015, **48**, 1152-1161.
27 D. A. Christian, A. Tian, W. G. Ellenbroek, I. Levental, K. Rajagopal, P. A. Janmey, A. J. Liu, T. Baumgart and D. E. Discher, *Nat. Mater.*, 2009, **8**, 843-849.
28 S. H. Han, V. Pryamitsyn, D. Bae, J. Kwak, V. Ganesan and J. K. Kim, *ACS Nano*, 2012, **6**, 7966-7972.
29 V. S. Kadam, E. Nicol and C. Gaillard, *Macromolecules*, 2012, **45**, 410-419.
30 F. C. Giacomelli, I. C. Riegel, C. L. Petzhold, N. P. da Silveira and P. Štěpánek, *Langmuir*, 2009, **25**, 731-738.
31 B. Charleux, G. Delaittre, J. Rieger and F. D'Agosto, *Macromolecules*, 2012, **45**, 6753-6765.
32 N. J. Warren and S. P. Armes, *J. Am. Chem. Soc.*, 2014, **136**, 10174-10185.
33 J.-T. Sun, C.-Y. Hong and C.-Y. Pan, *Polym. Chem.*, 2013, **4**, 873-881.
34 J.-T. Sun, C.-Y. Hong and C.-Y. Pan, *Soft Matter*, 2012, **8**, 7753-7767.
35 J. Rieger, *Macromol. Rapid Commun*. 2015, **36**, 1458-1471.
36 N. J. Warren, O. O. Mykhaylyk, A. J. Ryan, M. Williams, T. Doussineau, P. Dugourd, R. Antoine, G. Portale and S. P. Armes, *J. Am. Chem. Soc.*, 2015, **137**, 1929-1937.
37 Z. Liu, G. Zhang, W. Lu, Y. Huang, J. Zhang and T. Chen, *Polym. Chem.*, 2015, **6**, 6129-6132.
38 W.-J. Zhang, C.-Y. Hong and C.-Y. Pan, *Macromol. Rapid Commun.*, 2015, **36**, 1428-1436.
39 Y. Kang, A. Pitto-Barry, H. Willcock, W.-D. Quan, N. Kirby, A. M. Sanchezc and R. K. O'Reilly, *Polym. Chem.*, 2015, **6**, 106-117.
40 Y. Xu, Y. Li, X. Cao, Q. Chen and Z. An, *Polym. Chem.*, 2014, **5**, 6244-6255.
41 Q. Zhang and S. Zhu, *ACS Macro Lett.*, 2015, **4**, 755-758.
42 Y. Jiang, N. Xu, J. Han, Q. Yu , L. Guo, P. Gao, X. Lu and Y. Cai, *Polym. Chem.*, 2015, **6**, 4955-4965.
43 K. Bauri, A. Narayanan, U. Haldar and P. De, *Polym. Chem.*, 2015, **6**, 6152-6162.
44 W.-J. Zhang, C.-Y. Hong and C.-Y. Pan, *Macromolecules*, 2014, **47**, 1664-1671.
45 C. Gao, Q. Li, Y. Cui, F. Huo, S. Li, Y. Su and W. Zhang, *J. Polym. Sci., Part A: Polym. Chem.*, 2014, **52**, 2155-2165.
46 X. Zhang, J. Rieger and B. Charleux, *Polym. Chem.*, 2012, **3**, 1502-1509.
47 B. Karagoz, L. Esser, H. T. Duong, J. S. Basuki, C. Boyer and T. P. Davis, *Polym. Chem.*, 2014, **5**, 350-355.
48 C. A. Figg, A. Simula, K. A. Gebre, B. S. Tucker, D. M. Haddleton and B. S. Sumerlin, *Chem. Sci.*, 2015, **6**, 1230-1236.
49 Y. Pei, J.-M. Noy, P. J. Roth and A. B. Lowe, *Polym. Chem.*, 2015, **6**, 1928-1931.
50 S. Dong, W. Zhao, F. P. Lucien, S. Perrier and P. B. Zetterlund, *Polym. Chem.*, 2015, **6**, 2249-2254.
51 W.-D. He, X.-L. Sun, W.-M. Wan and C.-Y. Pan, *Macromolecules*, 2011, **44,** 3358-3365.
52 L. A. Fielding, M. J. Derry, V. Ladmiral, J. Rosselgong, A. M. Rodrigues, L. P. D. Ratcliffe, S. Sugiharaef and S. P. Armes, *Chem. Sci*., 2013, **4**, 2081-2087.
53 Y. Pei and A. B. Lowe, *Polym. Chem.*, 2014, **5**, 2342-2351.
54 W. Zhao, G. Gody, S. Dong, P. B. Zetterlund and S. Perrier, *Polym. Chem.*, 2014, **5**, 6990-7003.
55 C. Gao, S. Li, Q. Li, P. Shi, S. A. Shah and W. Zhang, *Polym. Chem.*, 2014, **5**, 6957-6966.
56 D. Zehm, L. P. D. Ratcliffe and S. P. Armes, *Macromolecules*, 2013, **46**, 128-139.
57 X. Xiao, S. He, M. Dan, Y. Su, F. Huo and W. Zhang, *J. Polym. Sci. Part A: Polym. Chem.*, 2013, **51**, 3177-3190.
58 Y. Kang, A. Pitto-Barry, A. Maitland and R. K. O'Reilly, *Polym. Chem.*, 2015, **6**, 4984-4992.
59 A. Blanazs, J. Madsen, G. Battaglia, A. J. Ryan and S. P. Armes, *J. Am. Chem. Soc.*, 2011, **133**, 16581-16587.
60 K. E. B. Doncom, N. J. Warren and S. P. Armes, *Polym. Chem.*, 2015, DOI: 10.1039/c5py00396b.
61 N. Yeole, S. N. R. Kutcherlapati and T. Jana, *RSC Adv.*, 2014, **4**, 2382-2388.
62 J. G. E. M. Fraaije and G. J. A. Sevink, *Macromolecules*, 2003, **36**, 7891-7893.
63 H. de Brouwer, M. A. J. Schellekens, B. Klumperman, M. J. Monteiro and A. L. German, *J. Polym. Sci. Part A: Polym. Chem.*, 2000, **38**, 3596-3603.
64 C. L. McCormick and A. B. Lowe, *Acc. Chem. Res.*, 2004, **37**, 312-325.

For Table of Contents use only

Macro-RAFT agent mediated dispersion polymerization: the monomer concentration effect on the morphology of the in situ synthesized block copolymer nano-objects

Zhonglin Ding, Chengqiang Gao, Shuang Wang, Hui Liu and Wangqing Zhang*

Key Laboratory of Functional Polymer Materials of the Ministry of Education, Collaborative Innovation Center of Chemical Science and Engineering (Tianjin), Institute of Polymer Chemistry, Nankai University, Tianjin 300071, China.

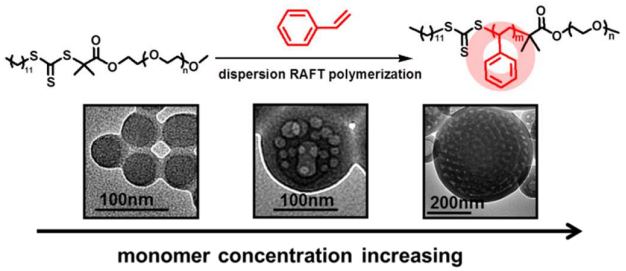

The great effect of the monomer concentration on the block copolymer morphology under dispersion RAFT polymerization is found and demonstrated.